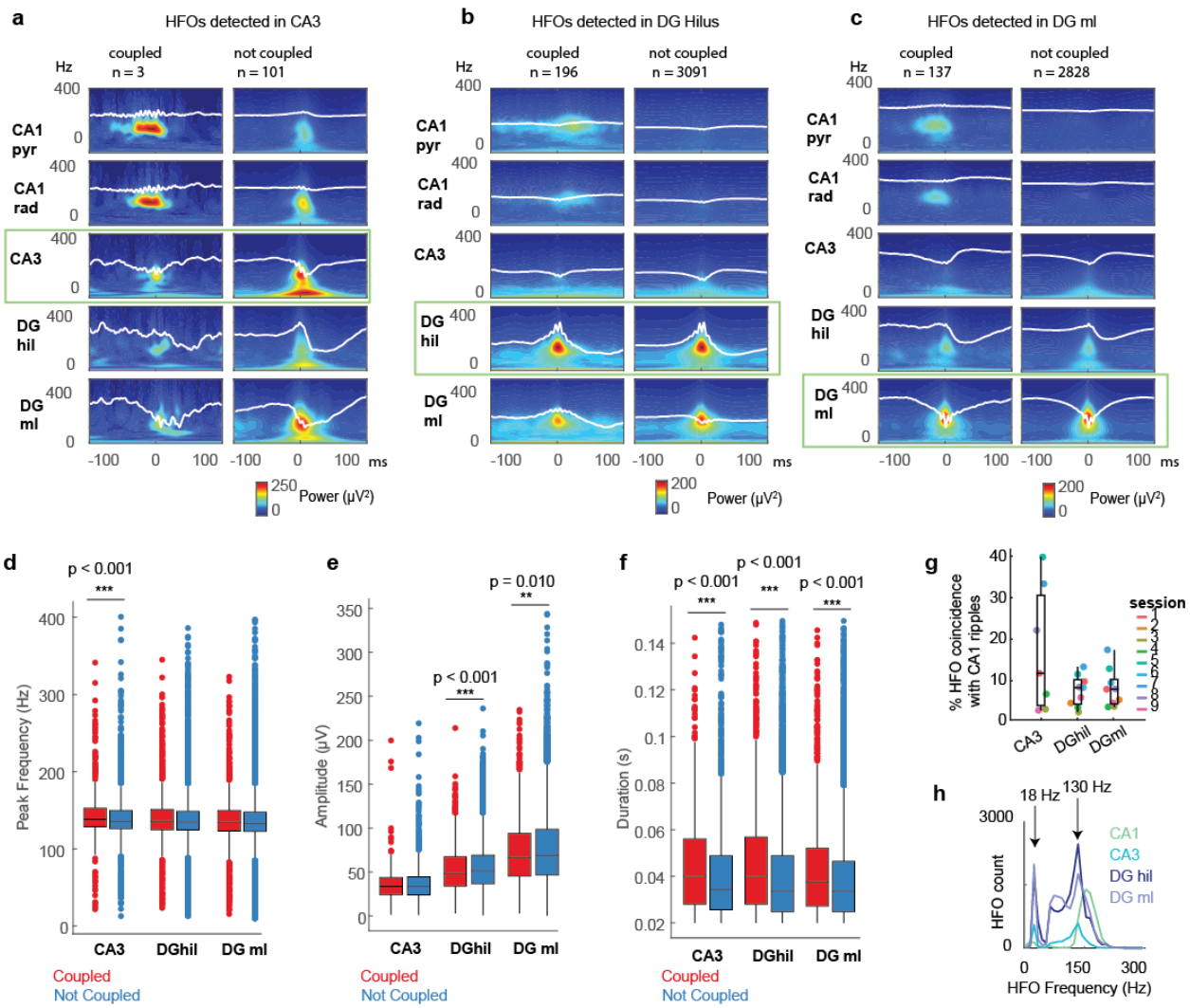

Supplementary Fig. 1: Events detected in mouse CA3 and DG using SPW-R-detection parameters are rarely coupled with CA1-SPW-Rs. **a** Average LFP traces and wavelet spectrograms of events (HFOs) detected on a CA3 channel from one recording session. The corresponding features computed on channels of different hippocampal subfields are shown: CA1 pyramidal layer (pyr), CA1 stratum radiatum (rad), CA3, DG hilus (hil) and DG molecular layer (ml). The detection channel is indicated by a green box. Left column: Events coupled to CA1-SPW-Rs (within ± 100 ms of the SPW-R peak in CA1). Right column: all other detections. **b** Same for detections in DG hilus. **c** same for detections in DG molecular layer. **d** Peak frequencies of events from all 5 mice detected in CA3 (n = 664 coupled vs. 2937 not coupled events, n sessions = 7), DG hilus (n = 1408 vs 15374 events, n sessions = 9) and DG molecular layer and coupled to CA1-SPW-Rs, compared to HFOs not-coupled to CA1-SPW-Rs; p-values were computed with Mann Whitney test. **e** Same for amplitudes of HFOs. **f** Same for HFO duration. **g**. Rates of coincidence of events detected in CA3, DG hilus and DG molecular layer with CA1 SPW-Rs. Coincidence was defined as both events being detected within ± 100 ms of the SPW-R peak in CA1. **h** Histogram of the peak frequencies of CA1 SPW-Rs and HFOs detected in different layers. Source data are provided as a Source Data file.

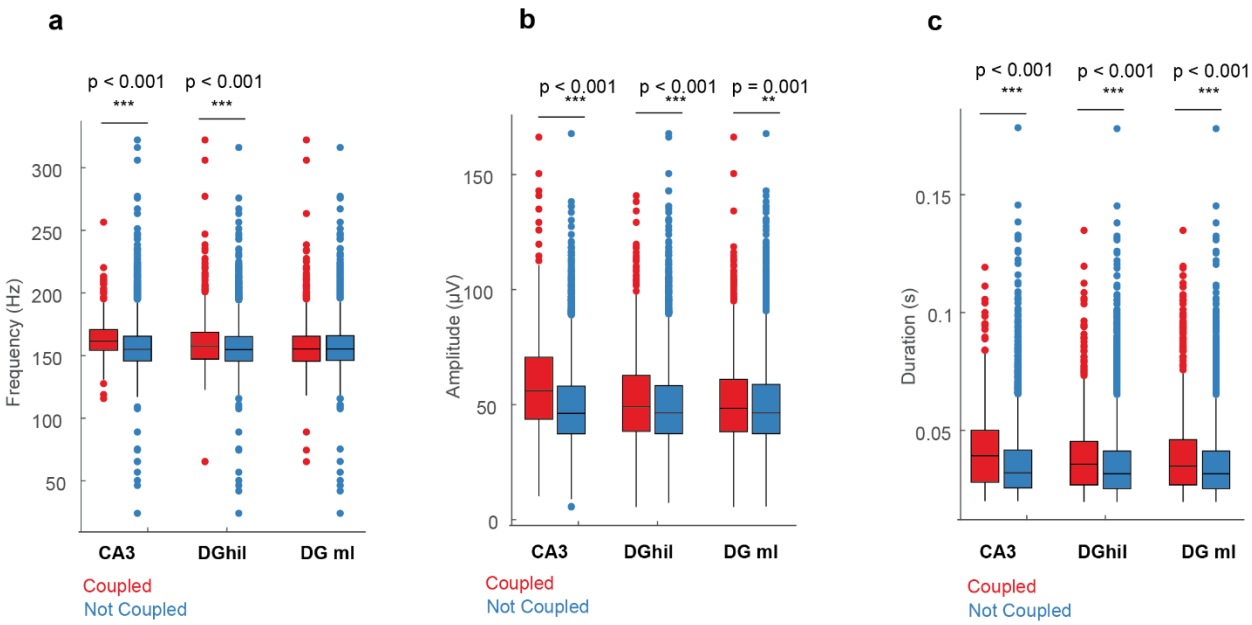

Supplementary Fig. 2: Features of mouse CA1 SPW-Rs coupled to events detected in other regions, compared to non-coupled SPW-Rs. a Peak frequency of SPW-Rs detected in CA1, and coupled to peaks in the ripple frequency band (HFOs) detected in CA3 (n = 652 vs 5863 uncoupled), DG hilus (n = 1379 vs 5755), or DG molecular layer, compared to peak frequencies of CA1-SPW-Rs not-coupled to peaks in other regions; p-values were computed with Mann Whitney test **b** Same for amplitudes of HFOs. **c** Same for HFO duration. Source data are provided as a Source Data file.

Region	Feature	(n)	Mean	Std	SEM	(n)	Mean	Std	SEM	Cohens_d	p_value*
Local events		Coupled				Not Coupled					
DG hilus	Amplitude (μV)	1408	52.49	25.92	0.69	15374	54.91	26.02	0.21	-0.09	0.0002
	Frequency (Hz)		139.99	32.64	0.87		137.93	30.05	0.24	0.07	0.07
	Duration (s)		0.046	0.024	0.001		0.040	0.020	0.000	**0.29**	1.56^{-24}
DG ml	Amplitude (μV)	1542	72.58	36.92	0.94	14814	76.34	40.94	0.34	-0.09	0.01
	Frequency (Hz)		136.54	33.59	0.86		136.14	34.64	0.28	0.01	0.21
	Duration (s)		0.043	0.02	0.00		0.039	0.019	0.000	**0.24**	5.04^{-19}
CA3	Amplitude (μV)	664	35.23	17.99	0.70	2937	36.05	18.64	0.34	-0.04	0.79
	Frequency (Hz)		143.38	32.99	1.28		139.96	30.12	0.56	0.11	0.0003
	Duration (s)		0.045	0.022	0.001		0.040	0.020	0.000	**0.24**	2.21^{-08}
CA1- SPW-Rs		Coupled				Not Coupled					
CA3	Amplitude (μV)	652	58.21	20.79	0.81	5863	49.02	17.17	0.22	**0.52**	2.01^{-36}
	Frequency (Hz)		163.18	14.72	0.58		157.05	17.22	0.22	**0.36**	2.98^{-18}
	Duration (s)		0.042	0.016	0.001		0.036	0.014	0.000	**0.42**	7.64^{-24}
DG hilus	Amplitude (μV)	1379	51.72	19.51	0.53	5755	49.26	17.42	0.23	0.14	4.53^{-06}
	Frequency (Hz)		159.71	18.77	0.51		156.64	16.60	0.22	0.18	2.16^{-09}
	Duration (s)		0.04	0.02	0.00		0.04	0.01	0.00	0.18	4.08^{-09}
DG ml	Amplitude (μV)	1503	51.05	18.47	0.48	5631	49.39	17.69	0.24	0.09	0.001
	Frequency (Hz)		157.12	17.80	0.46		157.27	16.89	0.23	-0.01	0.62
	Duration (s)		0.04	0.02	0.00		0.04	0.01	0.00	**0.22**	5.65^{-14}

Supplementary Table 1: Summary of event statistics. Local events: events from supplementary Fig 1, detected in DG hilus and molecular layer (ml) and CA3 and separated by their respective coupling to CA1-SPW-Rs, detected on a CA1 pyramidal channel. CA1-SPW-Rs – events detected in CA1 pyramidal layer, grouped by their coupling to CA3 and DG events – corresponding to supplementary Fig 2., *two-tailed Mann-Whitney U test

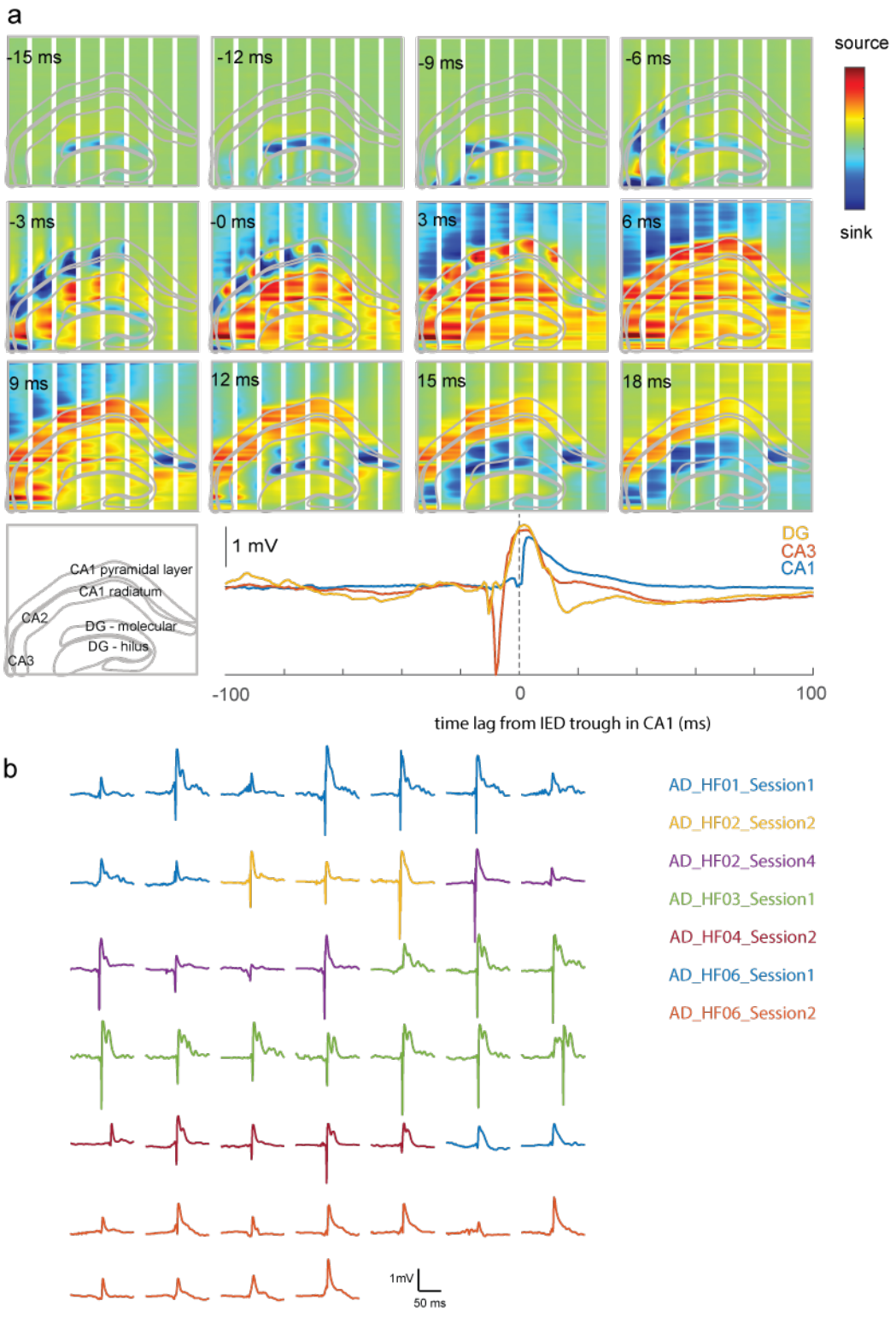

Supplementary Fig. 3: IEDs in APP/PS1 mice propagate along the hippocampal tri-synaptic circuit. **a** Example IED event propagation. Top: Current source density (CSD) maps calculated separately for each shank (128 channels per shank) over 2 ms time windows and timed to the negative spike in CA1 (dotted line on the bottom right plot). Note the initial current sink in the DG molecular layer (top left plot, at

-15 ms). Bottom left: layout of hippocampal subfield and layers Bottom right: LFP traces from three channels in DG (yellow), CA3 (orange) and CA1 (blue) **b** Waveforms of IEDs detected in the CA1 radiatum layer display high similarity within and across sessions. Different colors correspond to 7 different recording sessions from 5 APP/PS1 mice.

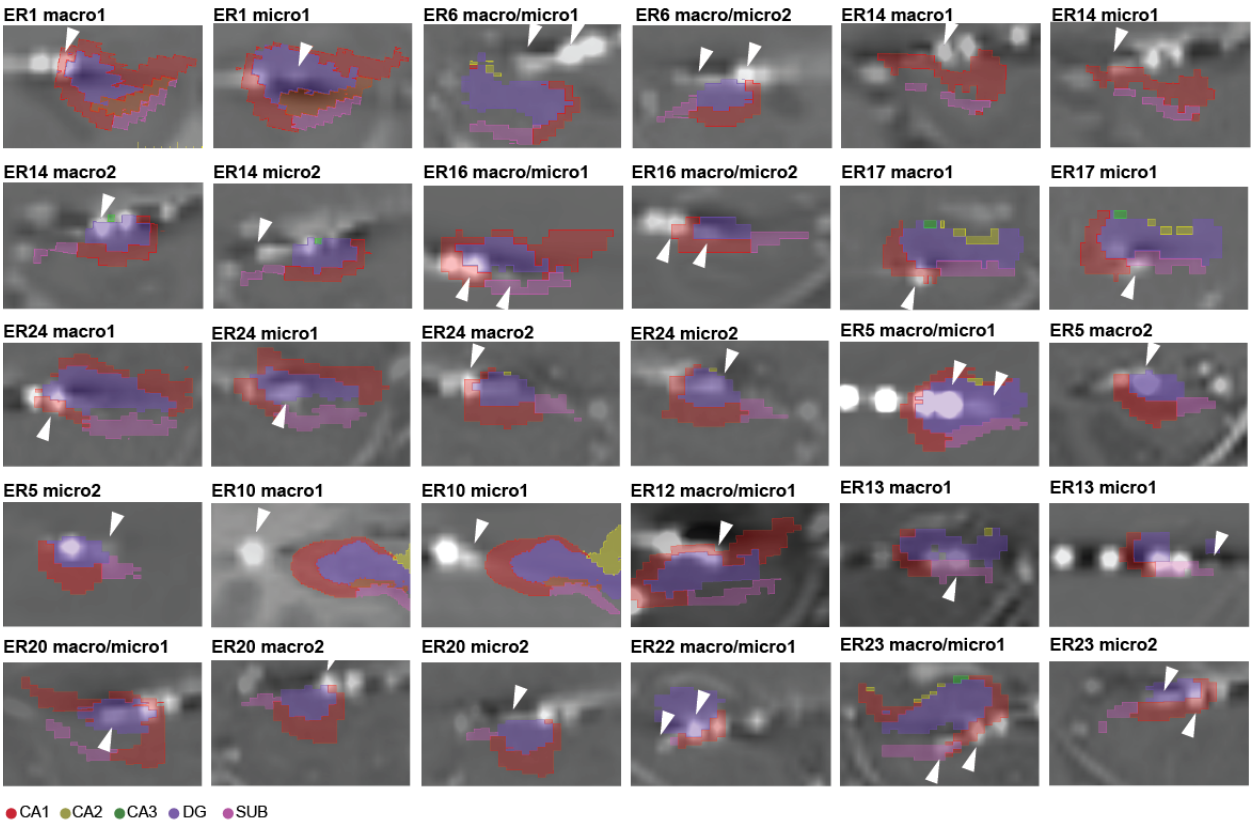

Supplementary Fig. 4: Location of human macrocontacts and microwires from all patients relative to hippocampal subfields. Each plot displays a coronal plane of the patient's postoperative CT-scan co-registered with a preoperative T1-MRI scan at the level of the respective depth electrode. The hippocampal subfield segmentation (ASHS, computed on the T2 MRI sequence) is superimposed on the anatomical images to identify the positions of macrocontacts and microwires (white arrowheads) with respect to the hippocampal subfields: CA1, CA2, CA3, dentate gyrus (DG) and subiculum (sub). Patient and contact are noted on top of each plot. Only contacts in the hippocampus are shown.

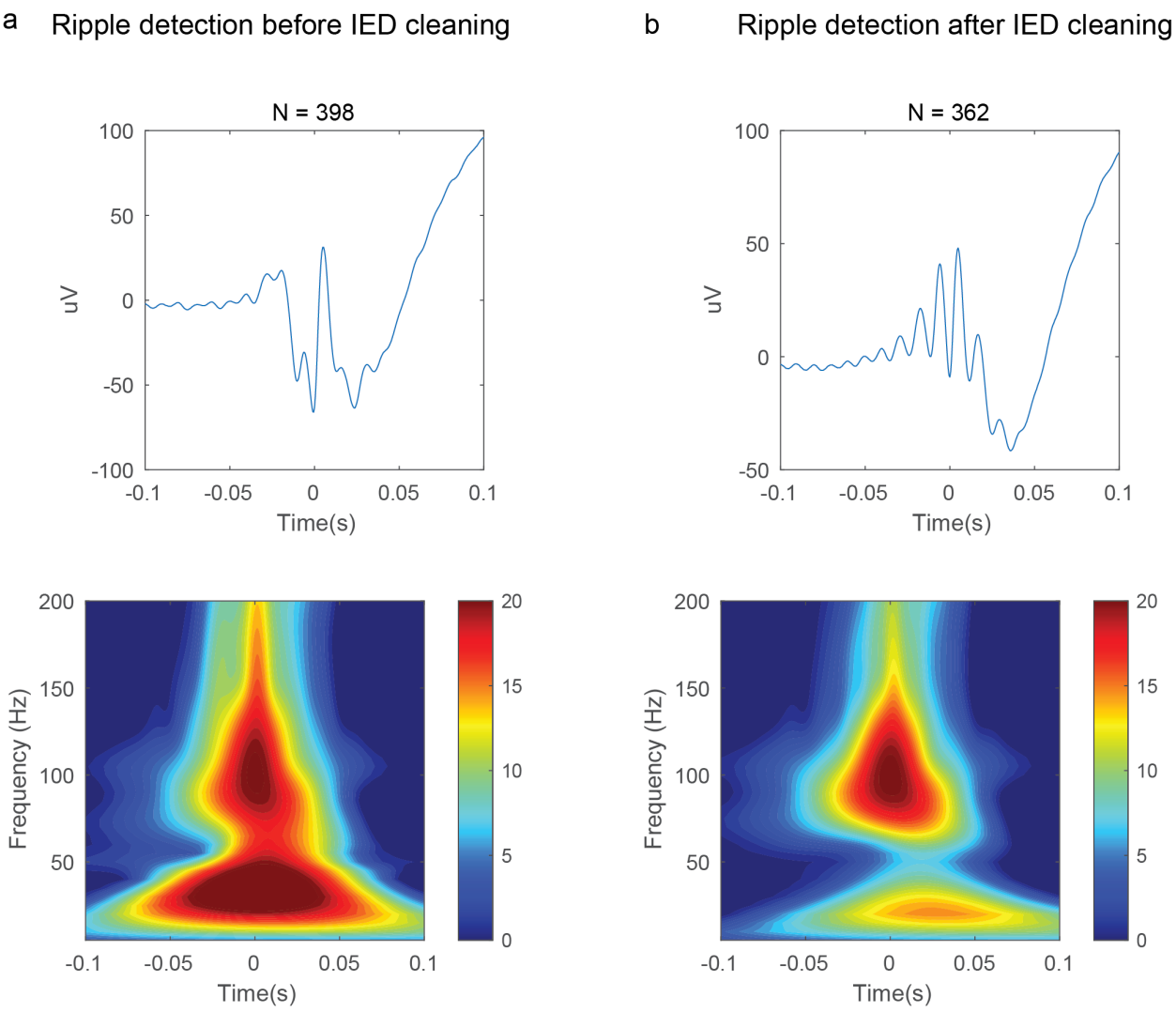

Supplementary Fig. 5: Discarding IEDs from the raw signal improves the accuracy of ripple detection. **a** Average LFP (top) and spectrogram (bottom) of automatically detected ripples from one example human channel. Most of these events were IEDs, obscuring true SPW-Rs. **b** Same as (a) but with removal of periods around IEDs (±0.5 s) from the signal before automatic ripple detection.

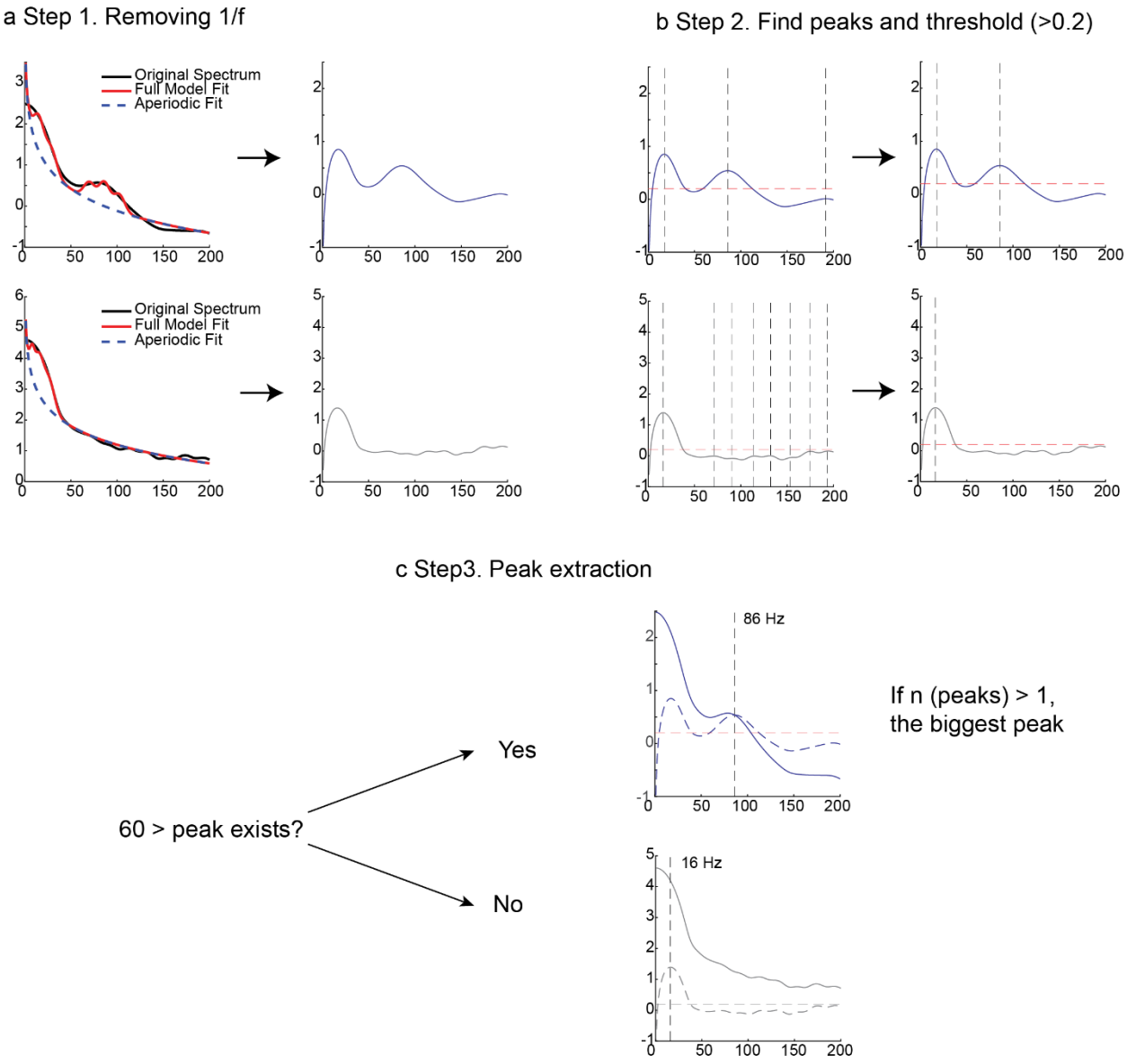

Supplementary Fig. 6: Spectral peak extraction from 1/f-corrected PSDs. a A 1/f-corrected PSD was obtained by subtracting the aperiodic component, fitted using FOOOF, from the original spectrum. **b** Peaks were identified from the 1/f-corrected PSD, and only those exceeding the threshold (0.2) were kept. **c** Among the detected peaks, a peak above 60 Hz was selected. If multiple peaks above 60 Hz were present, the largest peak was chosen. When no peak above 60 Hz was identified, the lower frequency peak was selected instead.

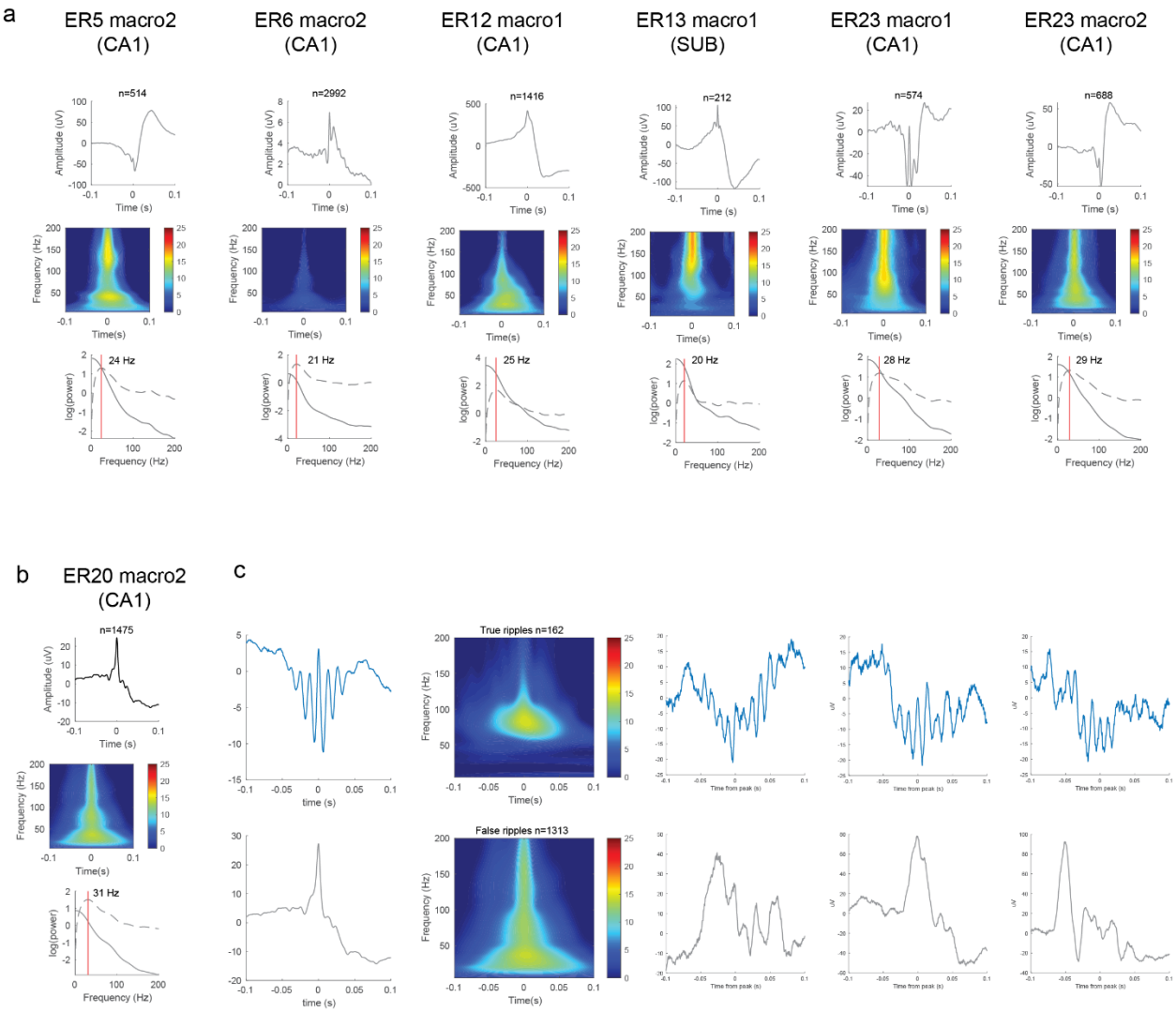

Supplementary Fig. 7. Human macrocontacts without >60 Hz spectral peak. a Average LFP waveforms, spectrograms and PSDs of automatically detected candidate ripples on macrocontacts without >60 Hz peak. **b** Same as (a) but for the only one ripple positive macrocontact. **c** True ripples (top) and false-positives (bottom) of the same channel as in (b). The true positive rate was 11%. Each row from left to right displays: average LFP waveform of all events, average spectrogram, three example events.

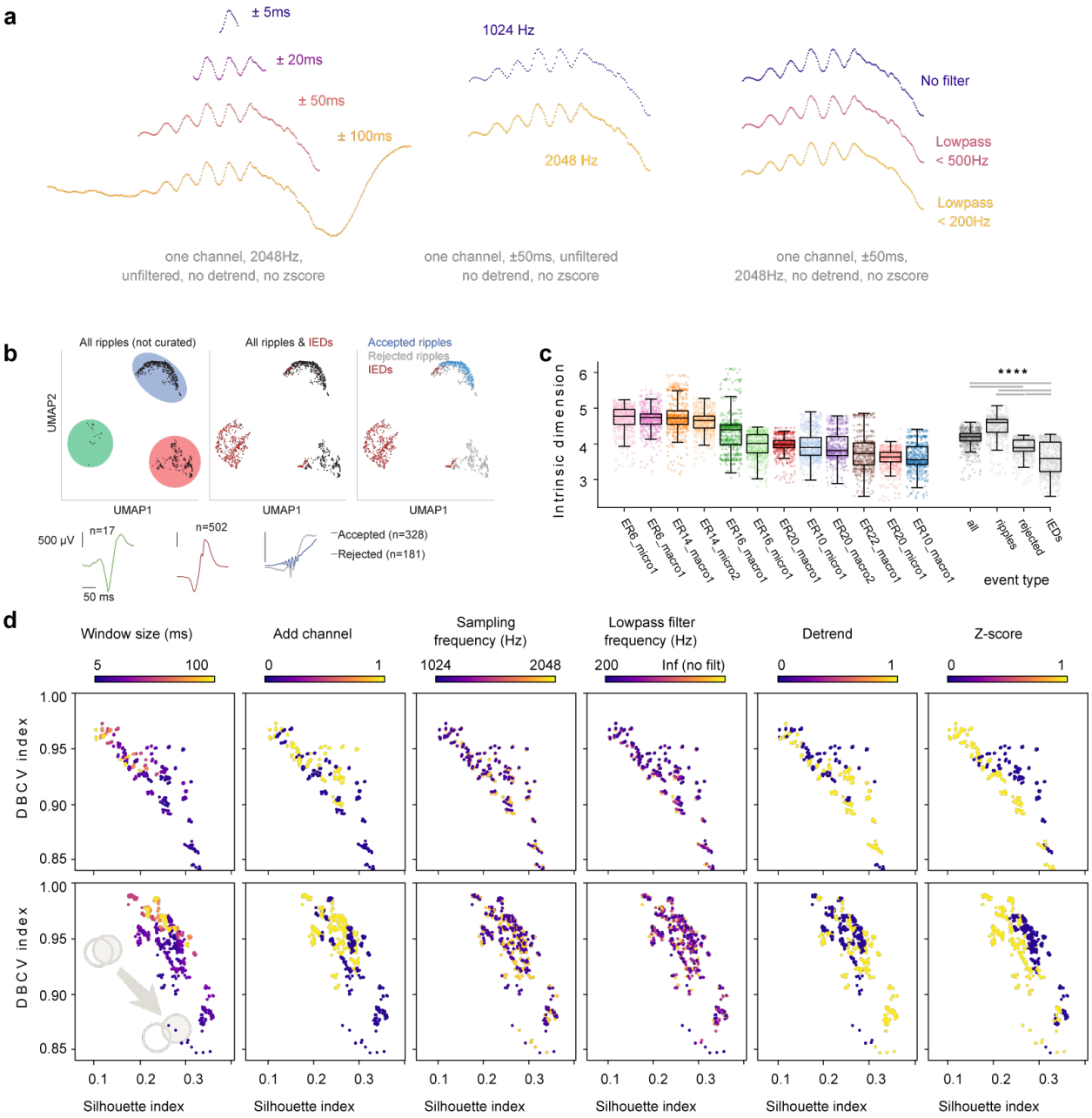

Supplementary Fig. 8: Topological characterization of events in the original and reduced spaces. a Examples of how events look like depending on different pre-processing characteristics. **b** Examples of manually inspected events in one channel used to validate and optimize UMAP separation. **LEFT:** UMAP projection of all automatically detected ripples and IEDs (n_neighbors=100, min_dist=0) from ER20 micro1. Dots in black represent the detected ripples (IEDs are not shown). Colored circles represent three distinct clusters of the events**. MIDDLE:** Same but including IEDs (red dots)**.** Note that some events project together with IEDs, potentially allowing their separation by UMAP before manual curation. **RIGHT:** Same clusters but ripples are color-coded by manually assigned labels from visual inspection. Blue: accepted, Grey: rejected. **BOTTOM:** Average waveforms of the three ripples clusters. The green and red colors correspond to the colors of the clusters in the top left plot. The blue cluster was manually curated, demonstrating the mixture of accepted (blue) and rejected events (gray) in this cluster. Note that the rest of the clusters near IEDs show IED-like waveforms. **c** Computing intrinsic dimension for all possible

combinations of parameters (window_size: ±5, ±10, ±15, ±20, ±25, ±50, ±75, ±100 ms; add_channel: True (1), by appending the LFP of an additional channel – the one that best optimized the metric for each case – after the event, or False (0), using only the selected HFO channel; sampling_frequency: 2048Hz, original, or 1024Hz, downsampled; lowpass_freq: no filtering, <500Hz, <400Hz, <300Hz, <200Hz; detrend: True, False; zscore: True, False). **LEFT:** Variability within and between sessions. **RIGHT:** Comparison of the intrinsic dimension between events labeled as “ripple”, “IED” or “FP” (false positives, or rejected ripples). All comparisons are significant, $p<0.00001$ (Kruskal-Wallis test with post hoc Dunn's test for multiple comparisons). FPs lie between the lower dimensionality of IED and higher of ripples. Mean intrinsic dimension of all events is 4D. **d** Mean clustering scores across sessions. We have used Density-Based Clustering Validation (DBCV) index and Silhouette indexes, very standard indexes to assess similarity between clusters. Low DBCV index and high Silhouette indicates good clustering. Here, each point represents the mean DBCV and Silhouette indices between the IED and ripple events of all sessions, for a particular set of pre-processing parameter combinations. Upper row: metrics computed in the original space, lower row: same in reduced space. Reducing the dimensionality preserves the structure of the mean scores. Source data are provided as a Source Data file.

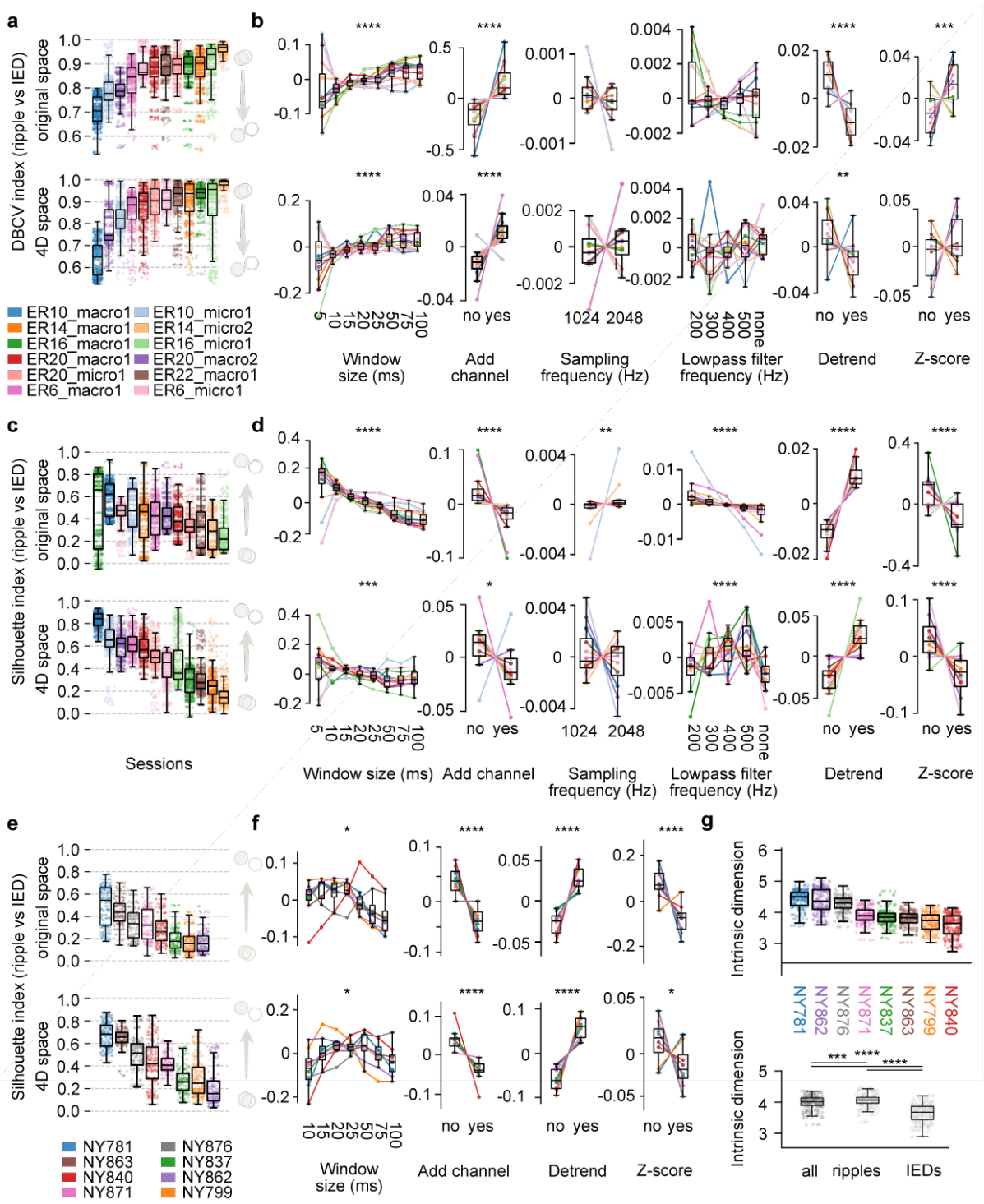

Supplementary Fig. 9: Snippet variables that optimize ripple-IED segregation. a. DBCV index to evaluate IED-ripple clustering per session, both in the original space (top) and the 4D space (bottom). Sessions have very different DBCV scores, indicating different levels of curation potential. Low DBCV index indicates good clustering. **b.** DBCV index changes depending on event features, in the original space (top) and the 4D space (bottom). Each line depicts the median of the cluster metric for a single patient for all possible values of the rest of the parameters. Add_channel describes whether the LFP of an additional channel was appended for computing the index (see also supplementary Fig 8c). Due to the

variability in the mean DBCV index across session, the mean score per session has been subtracted. Tendencies remain equal for the 4D space. **c,d.** Same as (a) and (b) but for the Silhouette index. Same conclusions. **e,f**. Same as (c) and (d) for an independent dataset of 8 patients/channels from a NYU Langone Epilepsy Center. Only significant results are shown. **g** Computing intrinsic dimensions for the patients/channels of the new dataset, for all possible combinations of parameters (same as in supplementary figure 8c). **TOP**: Variability within and between sessions. **RIGHT**: Comparison of the intrinsic dimension between all events, ripples and IEDs. Note significant differences in the dimensionality of ripples and IEDs. **b,d,f,g:** Stars indicate p-values of the statistical tests (ANOVA+Tukey for multiple comparisons in b,d,f or Kruskal-Wallis+Dunn in b,d,f,g, depending on the normality of the data): * p<0.05, ** p<0.01, ***p<0.005, ****p<0.001. For details see also Supplementary Tables 2:4. Source data are provided as a Source Data file.

Score	Space	Parameter	Comparison	p-value	Stars
DBCV	original	window_size	ANOVA+Tukey	0.00022	****
			0.005 vs 0.01	0.99998	
			0.005 vs 0.015	0.77658	
			0.005 vs 0.02	0.42223	
			0.005 vs 0.025	0.27569	
			0.005 vs 0.05	0.01277	*
			0.005 vs 0.075	0.0081	**
			0.005 vs 0.1	0.00418	***
			0.01 vs 0.015	0.92198	
			0.01 vs 0.02	0.63843	
			0.01 vs 0.025	0.46784	
			0.01 vs 0.05	0.03367	*
			0.01 vs 0.075	0.0222	*
			0.01 vs 0.1	0.01206	*
			0.015 vs 0.02	0.99933	
			0.015 vs 0.025	0.99247	
			0.015 vs 0.05	0.47301	
			0.015 vs 0.075	0.3819	
			0.015 vs 0.1	0.27046	
			0.02 vs 0.025	1	
			0.02 vs 0.05	0.81918	
			0.02 vs 0.075	0.73843	
			0.02 vs 0.1	0.60941	
			0.025 vs 0.05	0.92443	
			0.025 vs 0.075	0.87161	
			0.025 vs 0.1	0.77066	
			0.05 vs 0.075	1	
			0.05 vs 0.1	0.99997	

			0.075 vs 0.1	1	
		add_channel	ANOVA	0.00004	****
		sampling_frequency	Kruskal	0.52537	
		lowpass_freq	ANOVA	0.32363	
		detrend	ANOVA	0	****
		zscore	ANOVA	0.00328	***
	umap	window_size	ANOVA+Tukey	0.0003	****
			0.005 vs 0.01	0.96022	
			0.005 vs 0.015	0.41407	
			0.005 vs 0.02	0.11759	
			0.005 vs 0.025	0.0665	
			0.005 vs 0.05	0.00246	***
			0.005 vs 0.075	0.004	***
			0.005 vs 0.1	0.00301	***
			0.01 vs 0.015	0.96709	
			0.01 vs 0.02	0.69421	
			0.01 vs 0.025	0.54049	
			0.01 vs 0.05	0.06604	
			0.01 vs 0.075	0.09441	
			0.01 vs 0.1	0.07676	
			0.015 vs 0.02	0.99799	
			0.015 vs 0.025	0.98693	
			0.015 vs 0.05	0.51386	
			0.015 vs 0.075	0.60956	
			0.015 vs 0.1	0.55341	
			0.02 vs 0.025	1	
			0.02 vs 0.05	0.89256	
			0.02 vs 0.075	0.93885	
			0.02 vs 0.1	0.91374	
			0.025 vs 0.05	0.95968	
			0.025 vs 0.075	0.98163	
			0.025 vs 0.1	0.97029	
			0.05 vs 0.075	1	
			0.05 vs 0.1	1	
			0.075 vs 0.1	1	
		add_channel	ANOVA	0.00007	****
		sampling_frequency	ANOVA	0.41264	
		lowpass_freq	Kruskal	0.35858	
		detrend	ANOVA	0.00696	**

		zscore	ANOVA	0.10593	

Supplementary Table 2: Summary of statistics for Supplementary Fig. 9b

Score	Space	Parameter	Comparison	p-value	Stars
Silhouette	original	window_size	Kruskal+Dunn	0	****
			0.005 vs 0.01	0.74714	
			0.005 vs 0.015	0.40352	
			0.005 vs 0.02	0.05967	
			0.005 vs 0.025	0.00468	***
			0.005 vs 0.05	0.00005	****
			0.005 vs 0.075	0	****
			0.005 vs 0.1	0	****
			0.01 vs 0.015	0.24696	
			0.01 vs 0.02	0.02741	*
			0.01 vs 0.025	0.00163	***
			0.01 vs 0.05	0.00001	****
			0.01 vs 0.075	0	****
			0.01 vs 0.1	0	****
			0.015 vs 0.02	0.29471	
			0.015 vs 0.025	0.04625	*
			0.015 vs 0.05	0.0012	***
			0.015 vs 0.075	0.00011	****
			0.015 vs 0.1	0.00002	****
			0.02 vs 0.025	0.34452	
			0.02 vs 0.05	0.02845	*
			0.02 vs 0.075	0.00479	***
			0.02 vs 0.1	0.00126	***
			0.025 vs 0.05	0.21288	
			0.025 vs 0.075	0.06067	
			0.025 vs 0.1	0.02267	*
			0.05 vs 0.075	0.52858	
			0.05 vs 0.1	0.30151	
			0.075 vs 0.1	0.68693	
		add_channel	Kruskal	0.00003	****
		sampling_frequency	Kruskal	0.00558	**
		lowpass_freq	Kruskal+Dunn	0	****
			200.0 vs 300.0	0.38708	
			200.0 vs 400.0	0.00361	***
			200.0 vs 500.0	0	****

			200.0 vs 800.0	0	****
			300.0 vs 400.0	0.04081	*
			300.0 vs 500.0	0.00019	****
			300.0 vs 800.0	0.00002	****
			400.0 vs 500.0	0.09236	
			400.0 vs 800.0	0.02637	*
			500.0 vs 800.0	0.59082	
		detrend	ANOVA	0	****
		zscore	ANOVA	0.00039	****
	umap	window_size	Kruskal+Dunn	0.00125	***
			0.005 vs 0.01	0.93576	
			0.005 vs 0.015	0.92993	
			0.005 vs 0.02	0.16164	
			0.005 vs 0.025	0.04955	*
			0.005 vs 0.05	0.00363	***
			0.005 vs 0.075	0.00656	**
			0.005 vs 0.1	0.01272	*
			0.01 vs 0.015	0.99415	
			0.01 vs 0.02	0.13882	
			0.01 vs 0.025	0.04091	*
			0.01 vs 0.05	0.00279	***
			0.01 vs 0.075	0.00512	**
			0.01 vs 0.1	0.01011	*
			0.015 vs 0.02	0.13688	
			0.015 vs 0.025	0.0402	*
			0.015 vs 0.05	0.00273	***
			0.015 vs 0.075	0.00501	**
			0.015 vs 0.1	0.0099	**
			0.02 vs 0.025	0.5726	
			0.02 vs 0.05	0.13117	
			0.02 vs 0.075	0.18718	
			0.02 vs 0.1	0.27491	
			0.025 vs 0.05	0.34452	
			0.025 vs 0.075	0.4504	
			0.025 vs 0.1	0.59778	
			0.05 vs 0.075	0.8489	
			0.05 vs 0.1	0.67618	
			0.075 vs 0.1	0.8203	
		add_channel	ANOVA	0.02848	*
		sampling_frequency	ANOVA	0.3099	
		lowpass_freq	ANOVA+Tukey	0.00063	****

			200.0 vs 300.0	0.18217	
			200.0 vs 400.0	0.09613	
			200.0 vs 500.0	0.01178	*
			200.0 vs 800.0	0.98445	
			300.0 vs 400.0	0.99803	
			300.0 vs 500.0	0.79099	
			300.0 vs 800.0	0.05786	
			400.0 vs 500.0	0.92275	
			400.0 vs 800.0	0.02664	*
			500.0 vs 800.0	0.00245	***
		detrend	ANOVA	0	****
		zscore	ANOVA	0.00037	****

Supplementary Table 3: Summary of statistics for Supplementary Fig. 9d

Score	Space	Parameter	Comparison	p-value	Stars
Silhouette	original	window_size	Kruskal+Dunn	0.0268	*
			0.01 vs 0.015	0.35772	
			0.01 vs 0.02	0.39067	
			0.01 vs 0.025	0.4254	
			0.01 vs 0.05	0.65666	
			0.01 vs 0.075	0.28327	
			0.01 vs 0.1	0.05536	
			0.015 vs 0.02	0.95111	
			0.015 vs 0.025	0.9024	
			0.015 vs 0.05	0.17249	
			0.015 vs 0.075	0.04629	*
			0.015 vs 0.1	0.00457	***
			0.02 vs 0.025	0.95111	
			0.02 vs 0.05	0.1926	
			0.02 vs 0.075	0.05343	
			0.02 vs 0.1	0.00553	**
			0.025 vs 0.05	0.21438	
			0.025 vs 0.075	0.06147	
			0.025 vs 0.1	0.00666	**
			0.05 vs 0.075	0.5297	
			0.05 vs 0.1	0.14115	
			0.075 vs 0.1	0.39919	
		add_channel	ANOVA	0.00011	****
		sampling_frequency	Kruskal	0.09289	

		lowpass_freq	Kruskal	0.248	
		detrend	ANOVA	0.00000	****
		zscore	ANOVA	0.00044	****
	umap	window_size	ANOVA+Tukey	0.01784	*
			0.01 vs 0.015	0.2582	
			0.01 vs 0.02	0.04668	*
			0.01 vs 0.025	0.04636	*
			0.01 vs 0.05	0.04371	*
			0.01 vs 0.075	0.46871	
			0.01 vs 0.1	0.93307	
			0.015 vs 0.02	0.98516	
			0.015 vs 0.025	0.98489	
			0.015 vs 0.05	0.98245	
			0.015 vs 0.075	0.99974	
			0.015 vs 0.1	0.87432	
			0.02 vs 0.025	1	
			0.02 vs 0.05	1	
			0.02 vs 0.075	0.90276	
			0.02 vs 0.1	0.4105	
			0.025 vs 0.05	1	
			0.025 vs 0.075	0.90177	
			0.025 vs 0.1	0.40885	
			0.05 vs 0.075	0.89316	
			0.05 vs 0.1	0.395	
			0.075 vs 0.1	0.97662	
		add_channel	ANOVA	0.00019	****
		sampling_frequency	ANOVA	0.61036	
		lowpass_freq	ANOVA	0.61006	
		detrend	ANOVA	0	****
		zscore	ANOVA	0.03401	*

Supplementary Table 4: Summary of statistics for Supplementary Fig. 9f

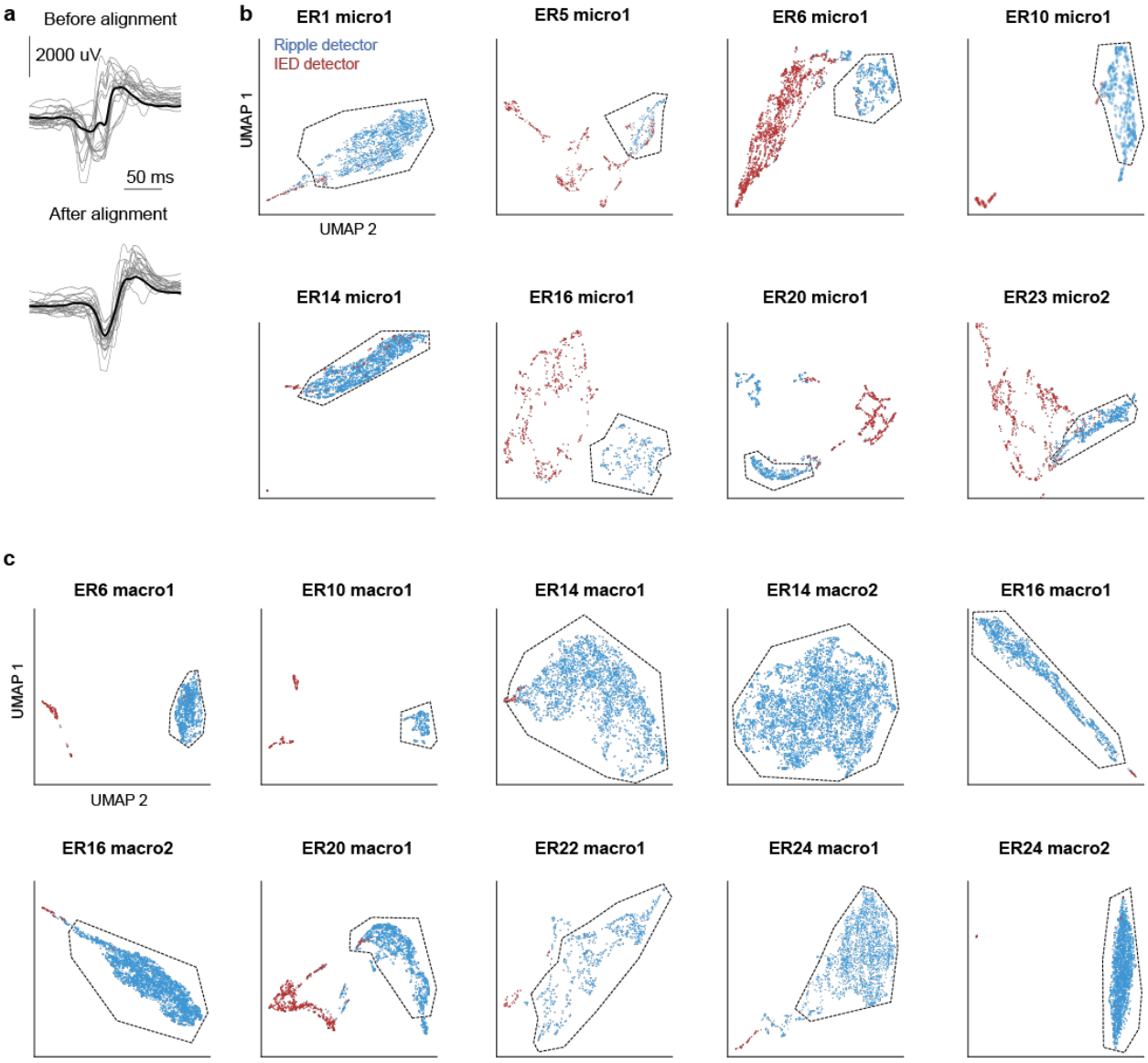

Supplementary Fig. 10: UMAP embedding of events detected on all human ripple-positive channels. a. Aligning IED peaks. **b.** UMAP embedding of events from microwires color-coded by detectors. Red: IED detector events, Blue: Ripple detector events. Dotted polygon indicates selected events for the next steps. **c.** Same as (b) but for macrocontacts.

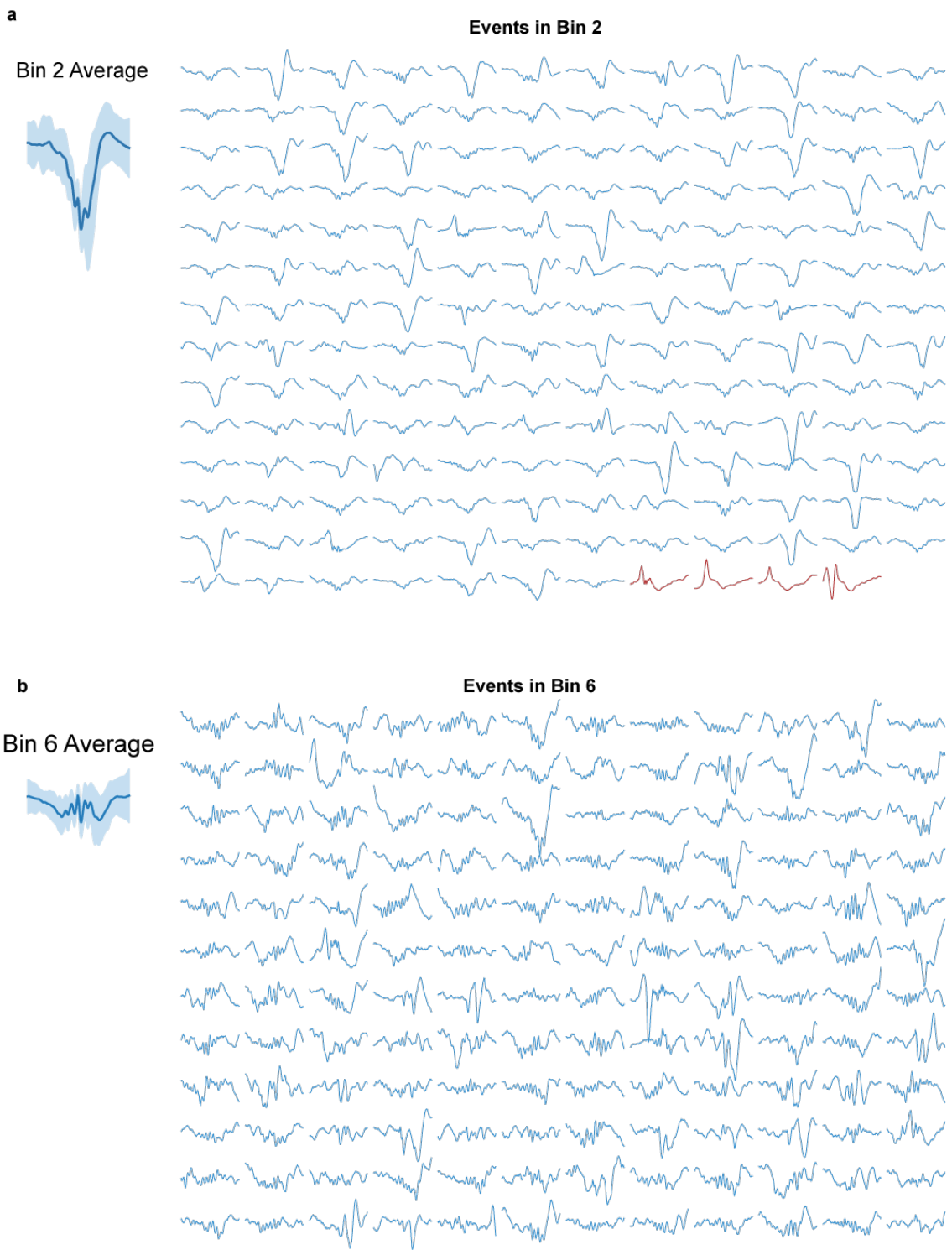

Supplementary Fig. 11: Importance of visualizing individual events for UMAP axis bin selection. a. LEFT, Average waveform of the events in Bin 2 in Fig. 4e. **RIGHT**, all the events in Bin 2. The average waveform of this Bin resembles ripples but many false-positives are included. **b.** Same as (a) but for Bin 6. This Bin contains many ripples but the average waveform is distorted by several false-positives with sharp waveforms.

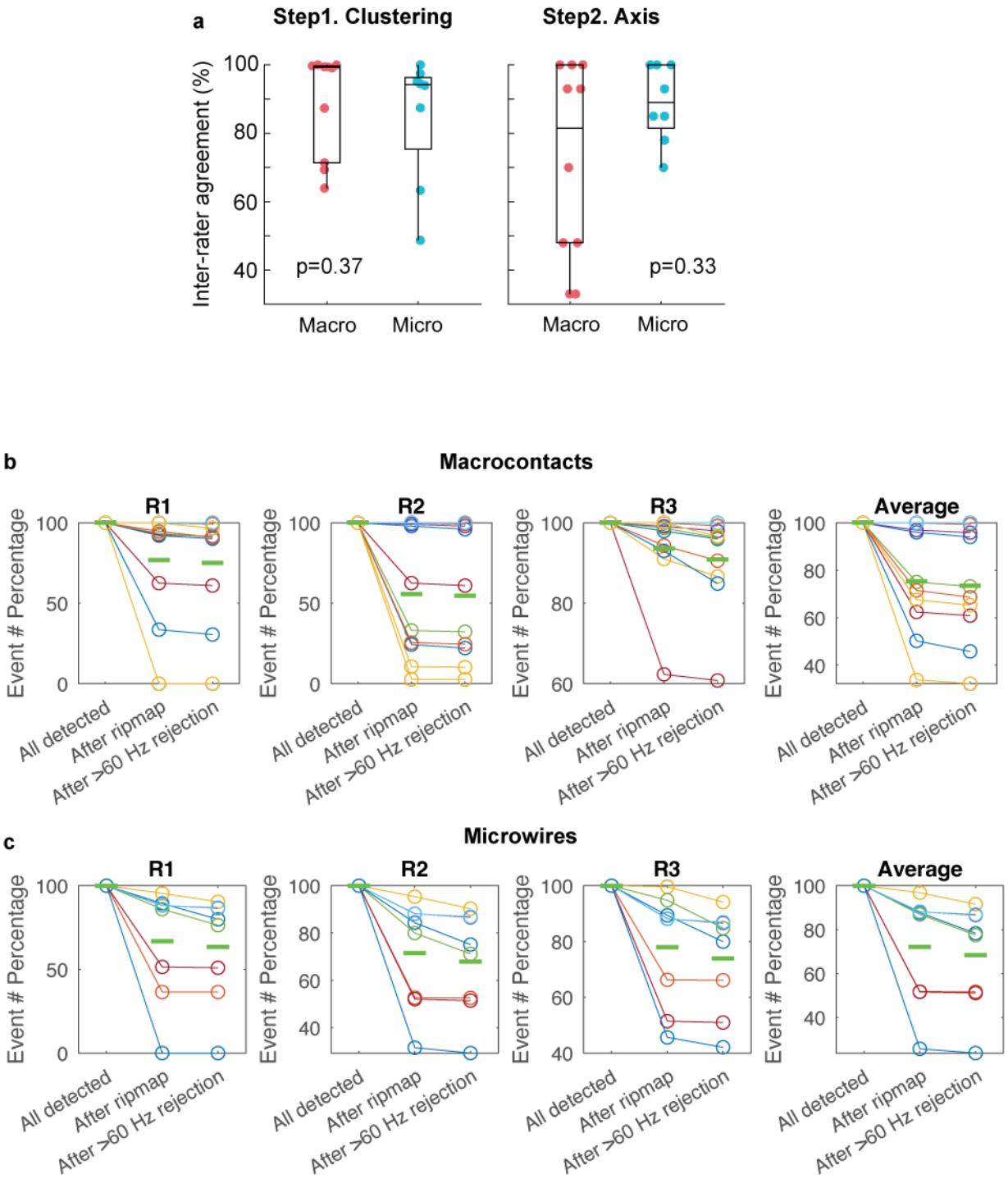

Supplementary Fig. 12: Ripmap performance and reproducibility. a. Inter-rater agreement (n=3 raters) for each ripmap step. Both clustering and axis steps show high inter-rater agreement, suggesting a high replicability of ripmap. There was no significant difference between macrocontacts and microwires (Wilcoxon rank-sum test, p>0.05) **b.** Percentage of accepted events in macrocontacts by each curation step. Circle colors correspond to a different channel. Green bars: means. **c.** Same as (b) but for microwires. Source data are provided as a Source Data file.

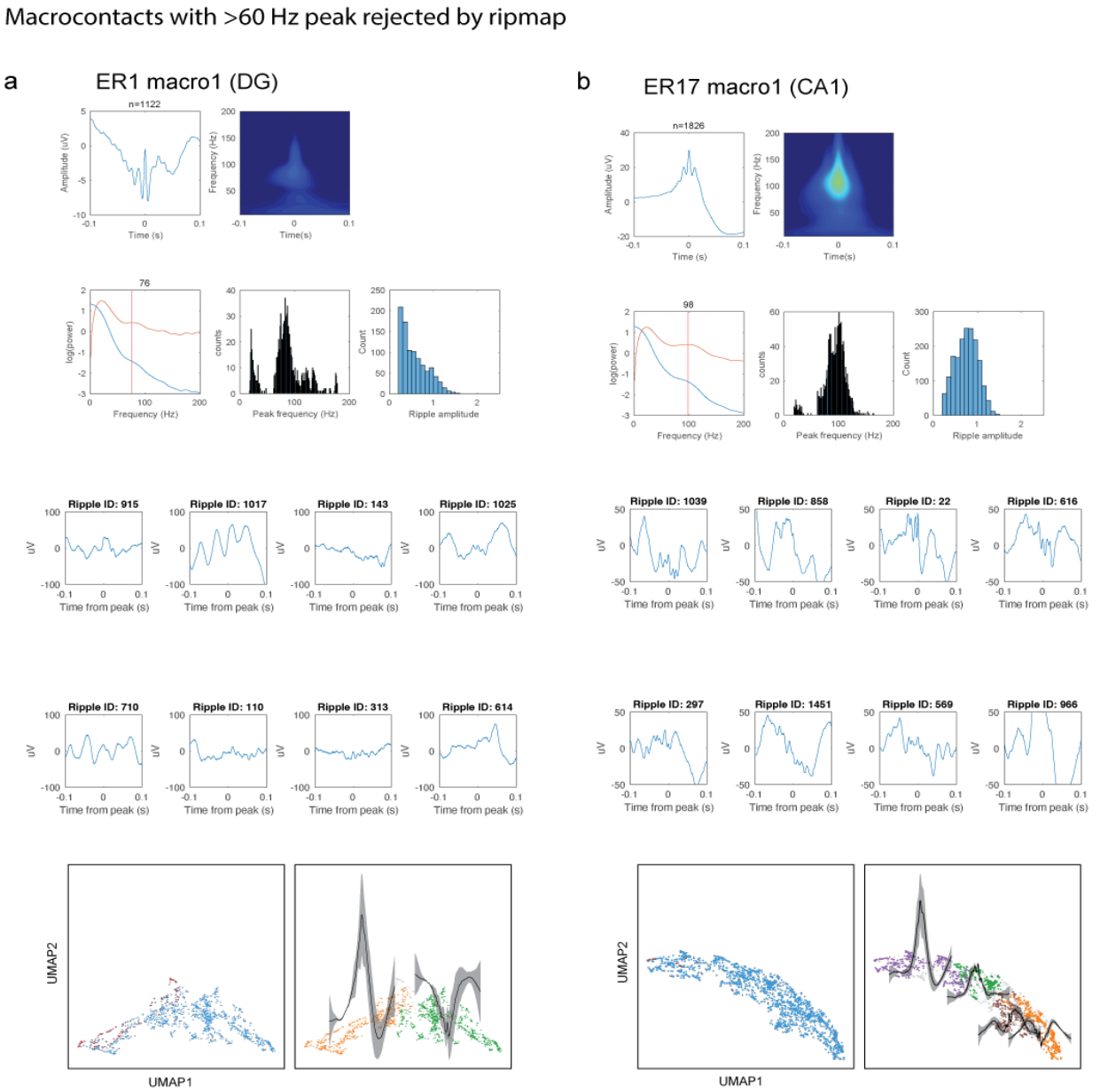

Supplementary Fig. 13: Human macrocontacts with >60 Hz spectral peak but rejected after ripmap. **a** Top: Average waveform, spectrogram, peri-event PSD, ripple peak distribution and ripple amplitude distribution for ER1 macro1. Middle: Example events. Bottom: UMAP result. **b.** Same as (a) but for ER17 macro1.

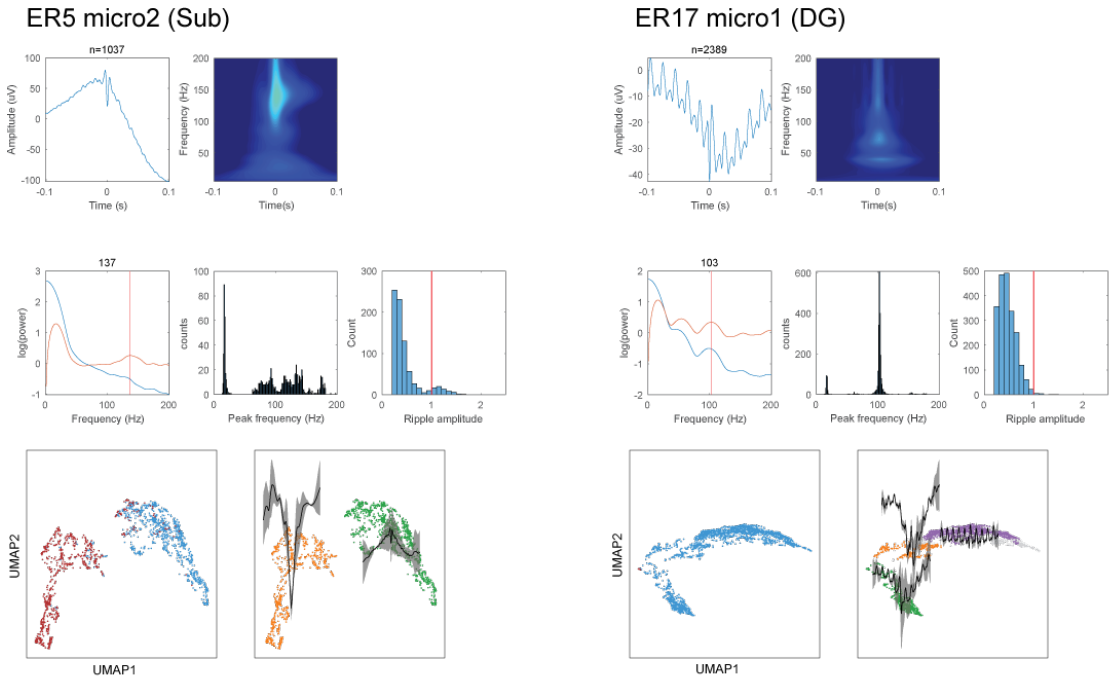

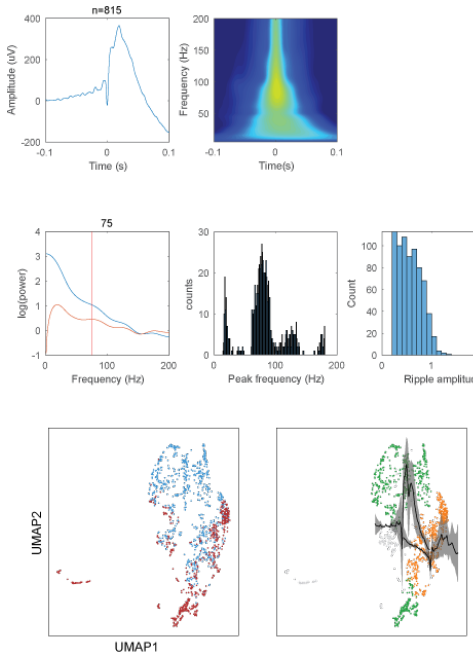

Supplementary Fig. 14: Human microwires with >60 Hz spectral peak but rejected after ripmap. a Top: Average waveform, spectrogram, peri-event PSD, ripple peak distribution and ripple amplitude distribution for ER1 macro1. Middle: Example events. Bottom: UMAP result.

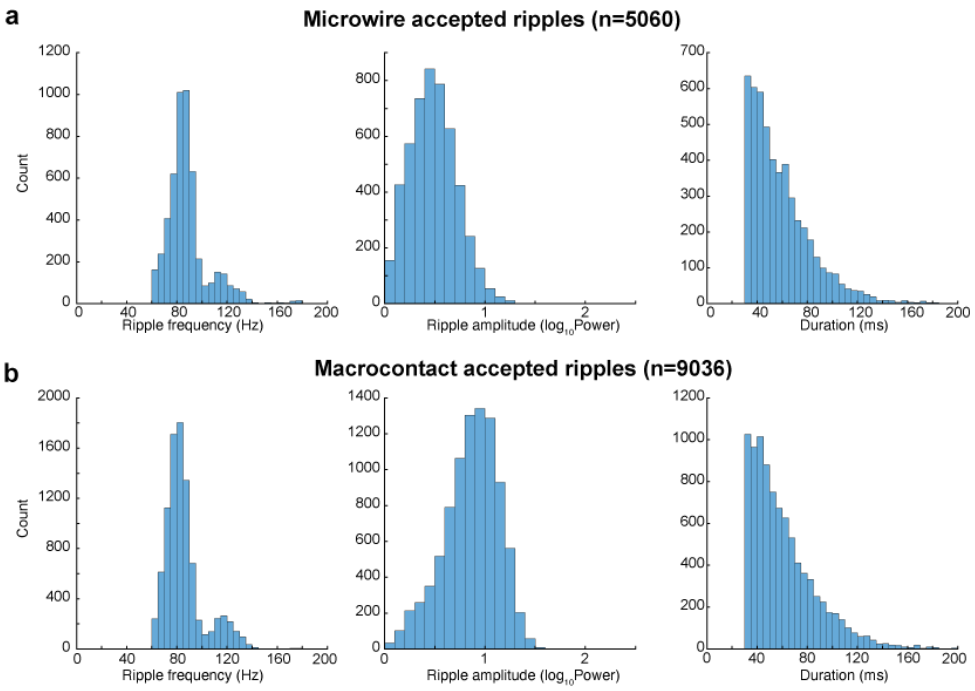

Supplementary Fig. 15: Ripple statistics: Peak frequency, amplitude, and duration distribution of ripples detected on microwires (a) and macrocontacts (b). Only consensus ripples from three raters were included for this analysis. Source data are provided as a Source Data file.

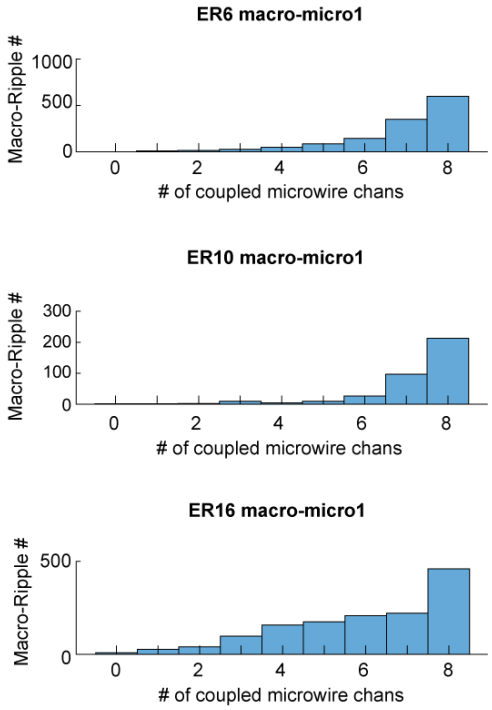

Supplementary Fig. 16: Number of coupled microwire channels during macrocontact ripples. The majority of macro-ripples are coupled with ripple activity on microwires. Only consensus ripples from three raters were included for this analysis. Source data are provided as a Source Data file.

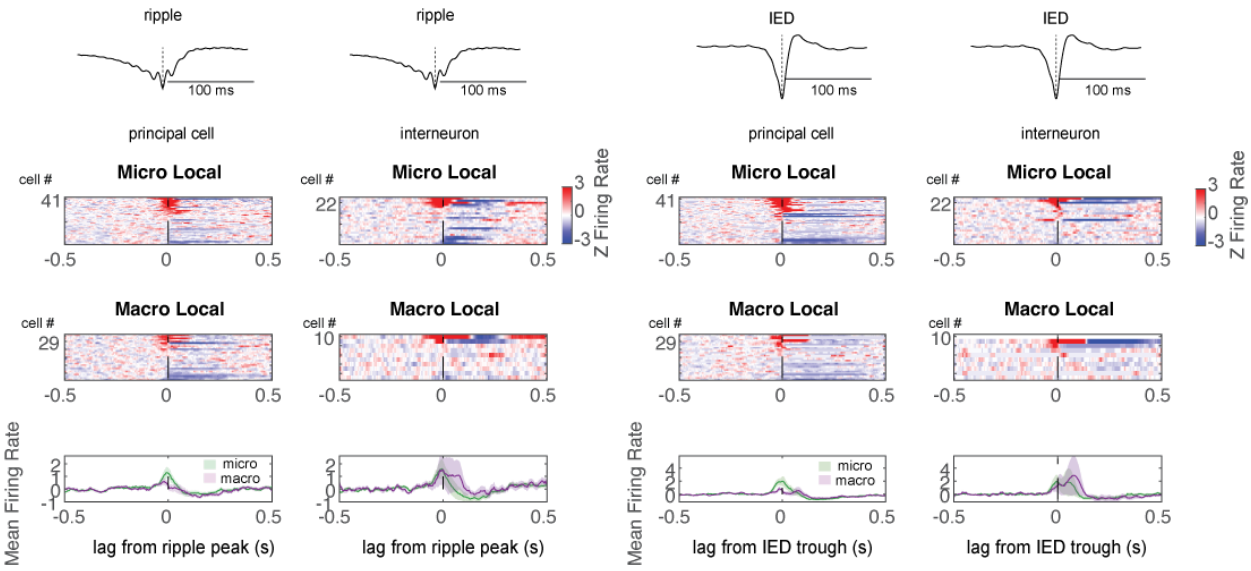

Supplementary Fig. 17: Peri-event PSTHs of human ripples and IEDs detected on microwire bundles and macrocontacts. Top: Example average LFP traces from one patient (ER6), centered to the negative ripple peak and IED peak respectively. **Middle:** Z-scored peri-ripple spiking in principal cells and interneurons in all 13 patients, time-locked to ripples and IEDs detected on the same microwire bundle (micro local) or the nearby macro-contact (macro local). **Bottom:** Mean z- scored firing rates (solid lines) and corresponding SEM (shaded) of neurons presented above. Source data are provided as a Source Data file.